The Journal of the Acoustical Society of America

OCTOBER 23 2026

Statistical models of Falcon 9 launch noise metrics at Vandenberg Space Force Base

Levi T. Moats ✉; Kent L. Gee ; Lucas K. Hall ; Grant W. Hart

Check for updates

J. Acoust. Soc. Am. 160, 3415–3427 (2026)
https://doi.org/10.1121/10.0046889

View Online Export Citation

Articles You May Be Interested In

Far-field acoustic variability across twelve Falcon 9 launches near Vandenberg Space Force Base
Proc. Mtgs. Acoust. (March 2026)

Overview and spectral analysis of the Falcon-9 SARah-1 launch and reentry sonic boom
Proc. Mtgs. Acoust. (October 2023)

Falcon 9 ascent sonic boom measurements in Ventura County, California
JASA Express Lett. (March 2026)

27 October 2026 16:38:30

ASA LEARN MORE
Advance your science and career as a member of the
Acoustical Society of America

ASA ACOUSTICAL SOCIETY OF AMERICA

JASA ARTICLE

Statistical models of Falcon 9 launch noise metrics at Vandenberg Space Force Base

Levi T. Moats,[1,a)] Kent L. Gee,[1] Lucas K. Hall,[2] and Grant W. Hart[1]
[1]*Department of Physics and Astronomy, Brigham Young University, Provo, Utah 84602, USA*
[2]*Department of Biology, California State University Bakersfield, Bakersfield, California 93311, USA*

ABSTRACT:
The Falcon 9 Block 5 is the world's most frequently launched orbital rocket, with 165 launches in 2025 alone. This cadence enables robust characterization of launch noise from repeated field measurements. This study analyzes 548 acoustic measurements from 76 Falcon 9 launches at Vandenberg Space Force Base (VSFB), spanning pad-to-station distances from approximately 230 m to 30 km. Mixed-effects models are developed to describe maximum sound level (L_{max}) and sound exposure level (SEL), including A- and C-weighted metrics, as functions of distance. Variability is modeled using a power-law variance structure, revealing increasing heteroskedasticity with distance. Prediction intervals derived from this structure quantify the range of expected individual measurements. Comparisons with Starship Super Heavy Flight 6 and launches from Florida suggest the model form is broadly applicable, though coefficients vary by vehicle. Additional analyses examine seasonal, diurnal, and terrain effects. Seasonal and diurnal effects are small for the present dataset, whereas terrain shielding can produce systematic reductions in level. Overall, this work provides a statistically grounded description of Falcon 9 launch noise and its variability and establishes a measured reference dataset for evaluation and future development of launch-noise prediction models. © *2026 Acoustical Society of America.*
https://doi.org/10.1121/10.0046889

(Received 1 May 2026; revised 31 August 2026; accepted 27 September 2026; published online 23 October 2026)
[Editor: Con Doolan] Pages: 3415–3427

27 October 2026 16:38:30

I. INTRODUCTION

The Falcon 9 Block 5 is a medium- to heavy-lift orbital launch vehicle capable of delivering approximately 15 600 kg to low Earth orbit and 8300 kg to geostationary transfer orbit, as well as supporting crewed missions to the International Space Station (SpaceX, 2025; NASA, 2026). Its relatively low launch cost, high operational reliability, and flexible mission profile have made Falcon 9 the dominant orbital launch vehicle in recent years, accounting for at least half of global orbital launches in 2024 and 2025 (McDowell, 2026; OECD, 2019, 2023). Current projections indicate that this high launch cadence will continue for several years (FAA, 2024, 2025; FAA Department of the Air Force United States Coast Guard and National Aeronautics and Space Administration, 2025).

The plume from each Falcon 9 launch acts as a high-amplitude, broadband acoustic source with low peak frequency (Eldred, 1971; Lubert *et al.*, 2022; Gee *et al.*, 2024). The high amplitudes and low peak frequency allow this broadband signature to propagate long distances, with infrasound traveling hundreds or even thousands of kilometers (Pilger *et al.*, 2021). As a result, launch noise can produce significant acoustic disturbances at locations well beyond the immediate launch complex (McInerny, 1992, 1997). These disturbances may affect nearby communities, infrastructure, and ecologically sensitive regions (Guest and Slone, 1972; Ang *et al.*, 2024; Casiano, 2024).

Rocket launch acoustic events are commonly summarized using metrics such as maximum sound level (L_{max}) and sound exposure level (SEL), along with along with A- and C-weighted variants. These metrics reduce complex, time-varying pressure waveforms to scalar quantities and are widely used in environmental acoustics, community-noise assessment, and regulation (ISO, 2016; FAA, 2025). Although this reduction omits temporal and spectral detail, these metrics provide practical measures of acoustic magnitude for comparing launches and assessing potential impacts.

Despite the growing number of global orbital launches, publicly available empirical characterizations of launch noise as a function of distance remain limited. Many existing rocket noise prediction approaches use semi-empirical or physics-based models that use engine and vehicle parameters as inputs (Mathews and Gee, 2025; Lubert *et al.*, 2022; Eldred, 1971; Christian *et al.*, 2023), while field measurements are often restricted to a small number of launches or measurement locations (Mathews *et al.*, 2020; Gee *et al.*, 2025a; Hart *et al.*, 2022). The high operational cadence of Falcon 9 enables a complementary, data-driven approach to characterizing launch acoustics. Over the past eight years, researchers at Brigham Young University (BYU) have collected acoustic recordings from more than 75 Falcon 9 Block 5 launches using purpose-built data acquisition systems and commercial sound level meters with waveform

a)Email: lmoats@byu.edu

recording capability (Mathews *et al.*, 2020; Mathews *et al.*, 2021; Pulsipher *et al.*, 2024). The resulting spatially distributed dataset allows the mean behavior and variability of launch-noise metrics to be characterized over a wide range of distances.

This paper presents a statistical analysis of Falcon 9 launch noise using measurements collected at and around Vandenberg Space Force Base (VSFB). Mixed-effects models are developed for L_{max} and SEL metrics, along with their frequency-weighted variants using logarithmic distance and linear distance from the launch pad as predictors. The models characterize both the mean distance-dependent trend and the variability of individual measurements, including confidence intervals for the mean and prediction intervals for new observations. Because the fitted coefficients and uncertainty bounds are obtained entirely from measured data, the resulting models are statistical descriptions rather than physics-based propagation models. Their primary value is therefore as a reproducible reference dataset and statistical benchmark for evaluating existing launch-noise prediction approaches such as RUMBLE, LNM, and RNOISE. The data-driven formulation also limits direct extrapolation to other vehicles and measurement locations; these limitations are examined later in the paper.

The fitted coefficients from these models have useful physical interpretation. Their values resemble effects associated with source-level scaling, geometric spreading, and effective atmospheric attenuation effects that have been observed in pervious launch noise datasets. We therefore compare selected logarithmic decay coefficients with those from measurements from Starship Super Heavy Flight 6 to test whether aspects of the distance dependence are transferable across vehicles. We also examine terrain shielding using paired measurement locations approximately 3 km from the launch pad. These analyses are intended to identify which features of the statistical model may generalize and which appear to depend on vehicle.

II. MEASUREMENT DATASET AND INSTRUMENTATION

Acoustic measurements of Falcon 9 launch noise were collected opportunistically over approximately eight years at VSFB, with more than 90% of the measurements collected during the last three years. All measured Falcon 9 launches at VSFB launched from Space Launch Complex 4E. The dataset spans 76 Falcon 9 Block 5 launches and 75 measurement locations, with station distances ranging from approximately 200 m to 30 km (Fig. 1). In total 548 launch recordings were collected. Because the measurement locations were not originally selected as part of a single planned experiment, the sampling is spatially nonuniform; this limitation is addressed through clustering and random effects in the statistical model. Some sites were occupied during multiple launches. Portions of the dataset have been analyzed previously, including measurements from three launches at stations between 7 and 14 km from the pad (Mathews *et al.*, 2020; Mathews *et al.*, 2021), measurements from a single site approximately 8 km from the pad across multiple launches (Pulsipher *et al.*, 2024), and measurements from 2 launches measured each at 28 locations at distances from 0.2 to 38.6 km from the launch pad (Kellison *et al.*, 2026). The recordings analyzed in those studies are included in the present dataset.

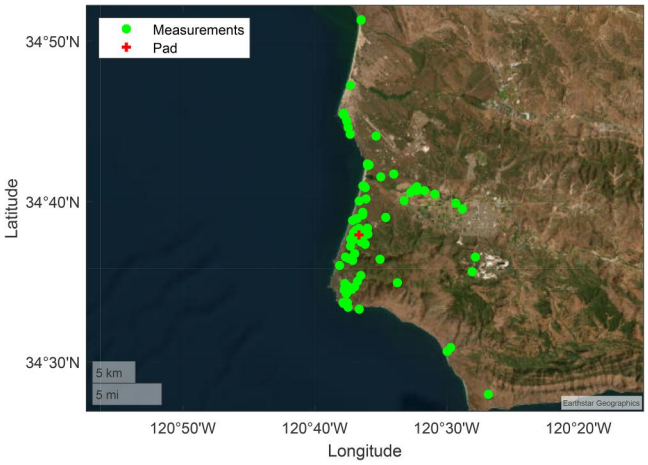


FIG. 1. A map of 75 measurement locations at VSFB where Falcon 9 launch noise was recorded. Falcon 9's launch pad (SLC-4E) is also shown.

A. Instrumentation and data acquisition

Acoustic waveform data were acquired using a combination of custom data acquisition systems and commercial sound level meters equipped with waveform recording capability. Microphones and acquisition systems were selected to accommodate the high-amplitude and low-frequency content characteristic of rocket launch noise. BYU-developed systems used 24-bit NI cDAQ hardware for data acquisition, including NI-9250, NI-9231, NI-9232, and NI-9234 modules depending on specific measurement goals. The microphones used were prepolarized GRAS microphones, including the 1/4" 46BG, 46BD, and 46BE models and the 1/2" 46AO, 46AE, 146AE and 47AC models. These systems have been used for many previous studies [e.g., Cunningham *et al.* (2023), Mathews *et al.* (2020), and Gee *et al.* (2025a)]. The specific microphone at a given location was selected so that dynamic range was never exceeded and signal-to-noise ratio was maximized. These systems were deployed for short periods of time ranging from one day to about a week. BYU-developed systems account for roughly half of records used in this study.

The commercial sound level meter solution used for these measurements was the Larson Davis 831C sound level meter with the optional waveform recording firmware. The frequency range for this system is compliant with IEC 61260:2014 Class 1 and ANSI S1.11–2014 Class 1 standards, providing a frequency response of 6.3 Hz to 20 kHz (Larson Davis, 2025). When appropriate, the microphone used for this system was PCB Piezotronics model 377B02. At locations closer to the rocket a Larson Davis half-to-quarter-inch adapter was used to fit a GRAS 40BD microphone onto the preamp to accommodate the higher

27 October 2026 16:38:30

https://doi.org/10.1121/10.0046889

amplitudes at that distance. The 831C meters were deployed for months at a time and routinely underwent maintenance, including calibration, in the field.

All systems were configured to record pressure waveforms sampled at 50, 51.2, or 102.4 kHz thus providing data that are suitable for post-processing into multiple acoustic metrics, including shock-related metrics (Pulsipher *et al.*, 2024). Instrumentation was deployed in outdoor locations, typically using BYU-developed ground-based windscreens previously characterized by Anderson *et al.* (2021, 2022). All microphones paired with BYU developed measurement equipment were deployed inverted such that the diaphragm was at a height of one diaphragm radius above a rigid ground plate place on a leveled spot of ground. A windscreen of acoustically transparent foam with a large outer radius was placed over the microphone. These deployments were all located in areas free of dense foliage, buildings, and other large reflecting or absorbing surfaces. Where necessary the ground was flattened to give the ground plate a smooth surface for deployment. All deployments guaranteed an unobstructed line of sight to the rocket at the angle of maximum acoustic radiation with the exception of a very limited dataset intentionally collected to investigate terrain shielding effects. The determination of whether a location had line of sight to the rocket was made using GIS data and an estimated angle of maximum acoustic radiation of 69° as calculated by Mathews *et al.* (2021) using the Ortel convective Mach number. This estimated angle of maximum acoustic radiation is also supported by more recent analysis by Gee *et al.* (2025a) where an angle of ∼70° is calculated using engine plume parameters to obtain the convective Mach number. The terrain-shielded recordings were only used in a comparative analysis presented at the end of this paper.

Microphone deployments using the 831C meter were made identically to those of the BYU developed measurement equipment with a few notable exceptions. Due to long term deployment combined with ground-based setups, microphones in sandy coastal areas were slowly buried causing low-fidelity data and eventually complete data loss. To remedy this, these microphones were deployed upright less than 0.3 m (1 ft) above the ground.

All microphones paired with BYU-developed measurement equipment were calibrated in the lab several days before deployment as well as day-of-launch using a GRAS 42AG calibrator. Calibration values were usually within 0.2 dB and never varied more than 0.5 dB between the lab and field. Long-term deployments were calibrated roughly every 2 weeks using a Larson Davis CAL250 calibrator. Changes in calibration for long-term deployments were monitored and did not exceed 0.2 dB. For all microphones, a GRAS 90AC calibration system is used periodically to check for changes in microphone response.

B. Data vetting and quality control

All recorded waveforms underwent a systematic vetting process prior to analysis. Recordings were inspected for evidence of hardware-related issues, including microphone damage, cable faults, electrical interference, and clipping resulting from insufficient dynamic range. The most common issue was clipping found in long-term-deployed sound level meters due to amplitudes being too high for the hardware. Measurements exhibiting such issues and any others were excluded from further analysis.

C. Data management and database structure

Vetted waveforms and associated metadata were stored in a relational database developed specifically for this project (Moats, 2026). The database links raw acoustic recordings with derived acoustic metrics, measurement location information, instrumentation details, and launch-specific metadata such as date and time. Storing data within a relational database enables consistent processing across launches and measurement sites, facilitates reproducibility of analyses, and supports efficient querying of large datasets.

III. METRIC DEFINITIONS

To compare launches and measurement locations quantitatively, each recorded pressure waveform was reduced to a set of standard acoustic metrics. The definitions below establish the quantities used throughout the analysis and clarify their relevance to rocket launch acoustics.

A. Maximum sound level

In this work, the maximum sound level (L_{max}) is defined as the highest one-second time-averaged sound level within the launch event. This metric characterizes the period of maximum sustained acoustic amplitude and is useful for assessing peak acoustic loading and short-duration disturbance. The calculation does not use the fast- or slow-weighted exponential time constants implemented by many sound level meters. However, Williams *et al.* (2025) showed for Falcon 9 data that a one-second average L_{max} is very similar to the slow-weighted L_{max} reported by a sound level meter.

B. Sound exposure level

Sound exposure level (SEL) quantifies the total acoustic energy delivered over the launch event. SEL complements L_{max} by accounting for the duration of the acoustic exposure. Near the launch pad, where L_{max} is greatest, the rocket traverses the angle of maximum acoustic radiation relative to the microphone rapidly, producing a short-duration, high-amplitude event. Farther from the launch pad, the corresponding event is lower in amplitude but persists for a longer time. A maximum-level metric does not capture this difference in exposure duration, whereas SEL integrates the acoustic energy over time.

C. Frequency-weighted metrics

In addition to unweighted (Z-weighted) metrics, frequency-weighted variants of L_{max} and SEL are computed using standard A- and C-weighting curves. A-weighting

27 October 2026 16:38:30

emphasizes frequencies to which human hearing is most sensitive at moderate sound levels, whereas C-weighting has a flatter response and retains substantially greater sensitivity to low frequencies. Thus, A-, C-, and Z-weighted metrics provide complementary descriptions of the launch-noise spectrum (IEC, 2013).

A-weighted metrics are widely used in environmental noise assessment and regulatory frameworks (FAA, 2022; OSHA, 2008; NIOSH, 1998). Because rocket launches contain substantial low-frequency energy, A-weighted metrics alone do not fully represent the physical acoustic environment. Accordingly, A-, C-, and Z-weighted variants are retained to support regulatory comparison while also characterizing the low-frequency content that is important for rocket noise.

IV. STATISTICAL MODEL DEVELOPMENT

The modeling objective is to characterize the distance dependence of L_{max} and SEL and their Z-, C-, and A-weighted variants using a reproducible statistical model based on data collected at VSFB. The dataset spans a wide range of propagation distances and includes measurements from many launches and locations, with potential variability associated with trajectory, terrain, and atmospheric conditions. A mixed-effects framework is therefore used to separate the dominant distance-dependent behavior from systematic and residual variability among measurements.

The model is intentionally streamlined. Rather than beginning with a highly parameterized description of all potentially relevant effects, the analysis first develops a model based on distance from the launch pad, which accounts for the dominant variation in the measured levels. The mean distance-dependent trend is estimated first, followed by confidence intervals for that mean and prediction intervals for individual observations. Additional predictors and alternative model structures are then evaluated to determine whether they provide sufficient improvement to justify increased model complexity. All equations and parameter values required to reconstruct the final mean curves and uncertainty intervals are provided in this section. Physical interpretation of the fitted parameters is deferred to the Results section.

A. Statistical framework and unit of replication

The dataset available for this analysis consists of 548 measurements collected across 76 launches at 75 distinct measurement locations. Because the measurements were collected opportunistically over several years rather than as part of a single planned experiment, the number and spatial distribution of measurements vary among launches and locations. A mixed-effects model provides a framework for representing the overall behavior common to the dataset while accounting for systematic variation among groups of observations.

Before fitting the model, the data were aggregated and clustered to establish an appropriate unit of replication and prevent nearly collocated measurements from artificially increasing the effective sample size. Some launches were recorded using multiple microphone channels at essentially the same location. Measurements from these channels were averaged prior to analysis so that each location contributed a single mean acoustic metric per launch. This reduced the 548 individual measurements to 401 observations.

Measurement locations were then grouped into spatial clusters based on distance from the launch pad. The clusters consist of 29 non-overlapping concentric distance bands spanning approximately 200 m to 30 km. The inner and outer bounds of each cluster were selected so that the maximum expected level difference due solely to spherical spreading within a cluster did not exceed 0.4 dB, while retaining at least two observations in each cluster. Figure 2 illustrates these distance-based clusters.

Measurements at similar distances from the launch pad may share persistent characteristics associated with terrain or trajectory. Cluster identity is therefore incorporated as a random effect variable in the mixed-effects model, allowing measurements within a cluster to share a systematic deviation from the overall distance-dependent trend. In this framework, fixed effects describe the trend common to all observations, while the cluster-level random effect accounts for systematic differences among groups of measurements that are not described by distance alone. The magnitude of this cluster-level variability does not affect calculation of the mean but does contribute to prediction interval calculation.

Under this structure, the unit of replication is the mean acoustic metric measured within a given cluster and launch. With the data structure established, the analysis begins with the simplest mean model considered adequate to describe the dominant behavior in the dataset: a model based only on distance from the launch pad.

B. Distance-based mean model

Distance from the launch pad produces the dominant variation in the measured acoustic levels across the dataset. The analysis therefore begins with a streamlined mean

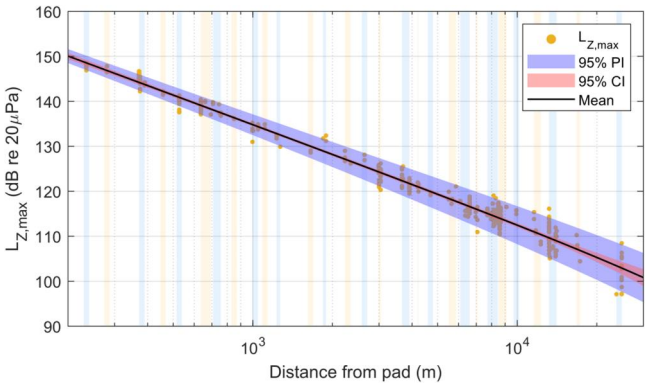


FIG. 2. Shown are 401 $L_{Z,max}$ data points each calculated from a measured Falcon 9 launch recording. Also, shown is a modeled mean, a confidence interval ($CI_{95\%}$) for the mean, and prediction intervals ($PI_{95\%}$) for new measurements taken at a random location. Alternating bands of color denote clustering of the data points.

27 October 2026 16:38:30

https://doi.org/10.1121/10.0046889

model in which distance is the only predictor. Additional variables and alternative model structures are discussed later.

Using the 401 observations described in Sec. IV A, the mean behavior of each acoustic metric is expressed as a function of distance r from the launch pad as

$$\mu(r) = \beta_0 + \beta_1 \log_{10}(r) + \beta_2 r, \tag{1}$$

where r is expressed in meters. In Eq. (1), the coefficients β_0, β_1, and β_2 are the fixed effects of the model and together define the mean function. The coefficient values for each metric are provided in Table I.

This same functional form is fit independently to each of the six acoustic metrics considered in this study. The resulting coefficients provide a reproducible description of the mean distance-dependent behavior over the measured range of approximately 200 m to 30 km.

C. Confidence intervals for the mean

Uncertainty in the fixed-effect coefficients β_0, β_1, and β_2 is summarized by their covariance matrix, denoted $\boldsymbol{V}$. This matrix is obtained from the mixed-effects model fit. The diagonal elements represent the variances of the individual coefficients, while the off diagonal elements represent covariances between coefficients. Values for the covariance matrix $\boldsymbol{V}$ for each acoustic metric is provided in Table II. The matrix indices correspond to the ordering of coefficients (β_0, β_1, β_2) in Eq. (1).

The standard error of the modeled mean at distance r is calculated using Eq. (2)

$$SE_\mu(r) = \sqrt{x(r)^T V\, x(r)}, \tag{2}$$

where $\boldsymbol{x}(r) = [1, \log_{10}(r), r]^T$ is the design vector evaluated at distance r. A 95% confidence interval for the mean is then constructed using Eq. (3) as

TABLE I. Curve coefficients used to calculate means using Eq. (1) and standard deviations using Eq. (5) and (6). The value σ_{cluster} is the standard deviation of the cluster random intercepts and is used in computing the predictive standard deviation σ_{pred} in Eq. (5). The parameters σ_0 and δ define the distance-dependent residual variability, where σ_0 sets the overall scale of the residual standard deviation and δ controls how that variability changes with distance. In Fig. 2 (and in other figures shown later for other metrics), the intercept term, β_0, sets the overall vertical position of the curve. The coefficient, β_1, captures the dominant distance-dependent reduction in level, i.e., geometric spreading. The final coefficient, β_2, allows the model to represent systematic long-range deviations from purely geometric decay; it serves as an empirical attenuation factor.

Metric	β_0	β_1	β_2	σ_{cluster}	σ_0	δ
$L_{Z,max}$	200.1	−21.8	−6.30E−05	0.58	0.071	2.43
$L_{A,max}$	186.3	−21.8	−9.34E−04	1.13	0.054	3.23
$L_{C,max}$	200.2	−22.7	−9.54E−05	0.54	0.049	2.89
ZSEL	193.9	−16.5	−2.71E−04	0.60	0.049	2.44
ASEL	191.3	−21.1	−8.39E−04	1.09	0.037	3.31
CSEL	194.5	−17.8	−3.42E−04	0.59	0.039	2.79

TABLE II. Covariance matrix elements of the fixed-effect coefficients used to compute the standard error in Eq. (2). The matrix is symmetric, so entries reflected about the diagonal are equal, as indicated in the column headers.

Metric	V_{00}	$V_{01} = V_{10}$	$V_{02} = V_{20}$	V_{11}	$V_{12} = V_{21}$	V_{22}
$L_{Z,max}$	2.03	−0.689	6.08E−05	0.238	−2.22E-05	2.84E−09
$L_{A,max}$	8.01	−2.75	2.59E−04	0.961	−9.50E-05	1.29E−08
$L_{C,max}$	2.18	−0.75	7.12E−05	0.263	−2.62E-05	3.59E−09
ZSEL	1.75	−0.589	4.98E−05	0.202	−1.80E-05	2.22E−09
ASEL	6.4	−2.18	1.97E−04	0.756	−7.20E-05	9.49E−09
CSEL	1.9	−0.644	5.68E−05	0.222	−2.07E-05	2.66E−09

$$CI_{95\%}(r) = \mu(r) \pm 1.96\, SE_\mu(r), \tag{3}$$

where $\mu(r)$ is computed using Eq. (1) and the coefficients in Table I. The factor 1.96 corresponds to the 97.5th percentile of the standard normal distribution and yields a two-sided 95% interval under the assumption of approximate normality of the predictive errors.

Because the dataset contains many observations distributed across the modeled distance range, the resulting confidence intervals are relatively narrow for all six acoustic metrics. This indicates that the mean distance-dependent trends are well constrained by the available data. Variability expected for individual observations however is much wider than the uncertainty in the mean. That variability is quantified by prediction intervals.

D. Prediction intervals for new observations

A prediction interval describes the range within which a single future observation at distance r is expected to fall. Unlike the mean function $\mu(r)$ defined in Eq. (1), which describes average distance-dependent behavior, a prediction interval characterizes the variability of individual measurements about that mean.

The residual variability in the dataset is not constant with distance. Instead, the spread of the residuals increases from approximately ±2 dB near the launch pad to approximately ±11 dB at the largest modeled distances. This heteroskedasticity indicates that individual measurements become progressively more variable with increasing range. Without explicitly accounting for this behavior, prediction intervals would incorrectly assume constant variability across all distances.

To represent this increase in variability, the residual standard deviation is modeled using a power-law variance structure shown in Eq. (4) as

$$\sigma_{\text{res}}(r) = \sigma_0 \left| \log_{10}(r) \right|^{\delta}, \tag{4}$$

where the parameters σ_0 and δ for each metric are estimated from the mixed effects model fit and provided in Table I. The parameter σ_0 represents a baseline scale of residual variability, while δ controls how rapidly that variability increases with distance.

Prediction uncertainty also includes systematic variability among the distance-based clusters defined in Sec. IV A.

27 October 2026 16:38:30

Each cluster is permitted to shift slightly upward or downward relative to the global mean curve through a random intercept. The magnitude of these cluster-level deviations is summarized by σ_{cluster}, which is the standard deviation of the random intercepts about the global mean. This term represents the systematic variability among groups of measurements that is not explained by distance alone.

The total predictive standard deviation at distance r combines the distance-dependent residual variation with the cluster-level variation as shown in Eq. (5)

$$\sigma_{\text{pred}}(r) = \sqrt{\sigma^2_{\text{cluster}} + \sigma^2_{\text{res}}(r)}. \tag{5}$$

A 95% prediction interval is then constructed using Eq. (6) as

$$PI_{95\%}(r) = \mu(r) \pm 1.96\, \sigma_{\text{pred}}(r), \tag{6}$$

where $\mu(r)$ is computed using Eq. (1) and the coefficients in Table I. The factor 1.96 corresponds to the 97.5th percentile of the standard normal distribution and yields a two-sided 95% interval under the assumption of approximate normality of the predictive errors.

Because $PI_{95\%}$ incorporates both cluster-level and distance-dependent variability, it is substantially wider than confidence intervals for the mean, particularly at larger distances. This distinction is important: the mean distance-dependent trend produced with the available data here is well constrained, while individual Falcon 9 measurements can still vary substantially about that trend. The following subsection evaluates whether additional predictors or alternative model structures explain a meaningful portion of this remaining variability.

E. Evaluation of additional predictors and model structures

The distance-based model developed in Secs. IV B–IV D captures the dominant trend in the measured acoustic levels while accounting for the observed increase in variability with range. However, distance is not expected to be the only physical factor that influences launch-noise measurements. Additional model terms were therefore evaluated to determine whether readily available information could explain a meaningful portion of the remaining variation and improve the model sufficiently to justify the added complexity. Candidate models were compared using Akaike's Information Criterion (AIC), for which smaller values indicate stronger support among the models considered (Akaike, 1974).

Alternative random-effects structures were considered. In addition to the distance-based cluster random effect described in Secs. IV A and IV D, individual launch mission was evaluated as a random effect to determine whether persistent launch-to-launch differences contributed meaningfully to the observed variability. The estimated mission-to-mission variability was negligible and did not improve model support. In contrast, inclusion of the distance-cluster random effect reduced AIC and provided a meaningful representation of systematic variation among measurement regions. The cluster random effect was therefore retained, whereas the mission-level random effect was excluded.

Potential temporal modulation of the mean was evaluated using circular representations of time of day and time of year. These terms were statistically significant in some comparisons, but the associated changes in modeled level were small, on the order of approximately 0.5 dB. For the present modeling objective, inclusion of the temporal terms increased the AIC relative to the distance-based mean model. The additional parameters therefore provided little practical improvement relative to their added complexity, and time of day and time of year were not retained as predictors of the modeled mean.

Payload mass and trajectory type were also considered as potential launch specific predictors. For the present dataset neither were proven to meaningfully explain the remaining variability of the modeled mean. Regarding payload mass this is not surprising as the maximum payload a Falcon 9 can put into orbit is only a small percentage, ~4%, of the total mass of the launch vehicle itself. Additionally, trajectories from VSFB are very similar for their first several kilometers of gained altitude, making the statistical insignificance of this variable also reasonable.

One variable that did make a statistically significant change in measured mean metric level was terrain shielding effects. As terrain shielding is a rare instance these data were excluded from the main model and are presented in Sec. VII.

These evaluations support retaining distance, r, as the sole predictor of the modeled mean while using the cluster random effect and distance-dependent variance structure to represent variability among individual observations. This choice should not be interpreted to mean that temporal, atmospheric, trajectory, terrain, or other propagation effects are physically unimportant. Rather, among the effects evaluated with the present dataset, no additional predictor produced sufficient improvement to warrant inclusion in the primary statistical model. The resulting model therefore retains a streamlined structure while leaving the remaining variability explicitly represented in its prediction intervals.

V. MODEL BEHAVIOR AND PHYSICAL INTERPRETATION

Mean values of L_{max} and SEL decrease monotonically with distance across the observed range. This behavior is consistent with expectations for an intense acoustic source subject to geometric spreading and additional distance-dependent attenuation. The fitted curves capture the dominant decay from approximately 200 m to 30 km, with no evidence of an abrupt regime change within the measurement range. The corresponding mean curves and uncertainty intervals for the unweighted, A-weighted, and C-weighted metrics are shown in Figs. 3–5. Weak long-range deviation from power law geometric spreading is present, particularly for $L_{A,max}$ in Fig. 4(a) and for the SEL plots in Figs. 3(b), 4(b),

27 October 2026 16:38:30

https://doi.org/10.1121/10.0046889

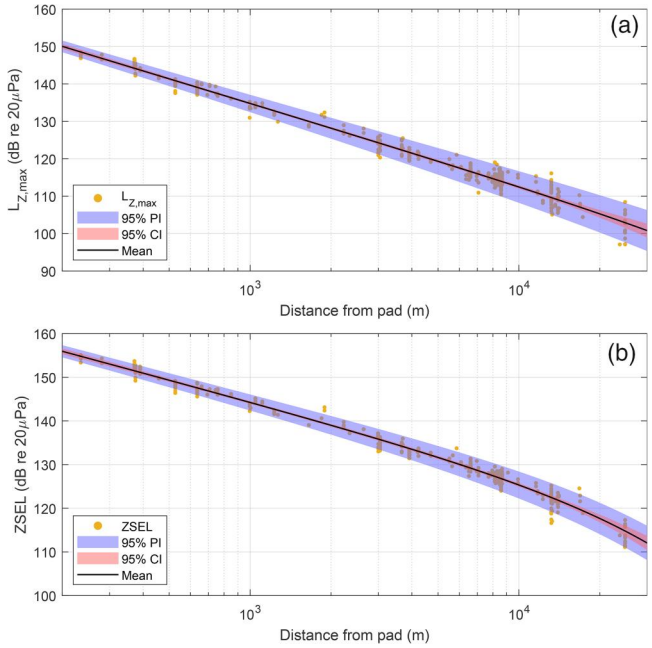


FIG. 3. The 401 $L_{Z,max}$ (a) and ZSEL (b) data points calculated from Falcon 9 launch recordings at VSFB, along with the modeled mean levels and the associated $CI_{95\%}$ and $PI_{95\%}$.

and 5(b). These losses that exceed those predicted by geometric spreading are represented by the β_2 term in Eq. (1).

A. Interpretation of mean model coefficients and variability parameters

The fitted coefficients permit limited physical interpretation, although they should not be treated as direct estimates of source or propagation parameters. The intercept, β_0, represents the extrapolated level at $r = 1$ m but this is not

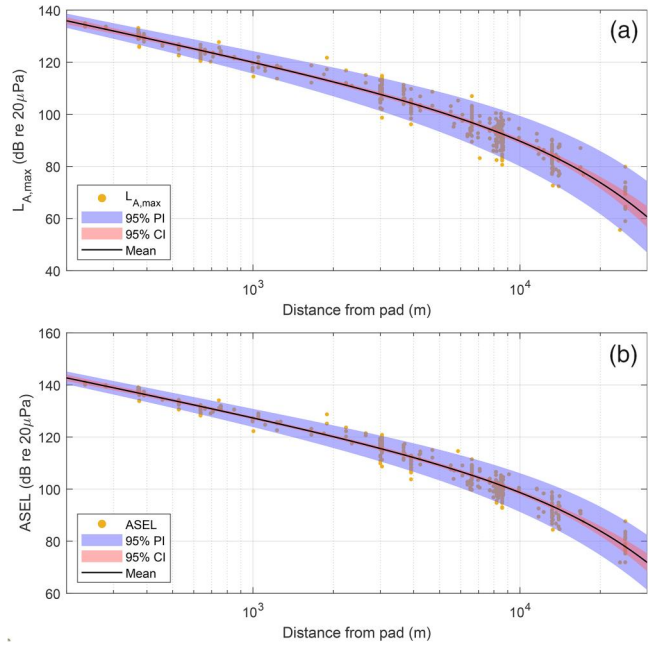


FIG. 4. Figure 3, but for A-weighted metrics.

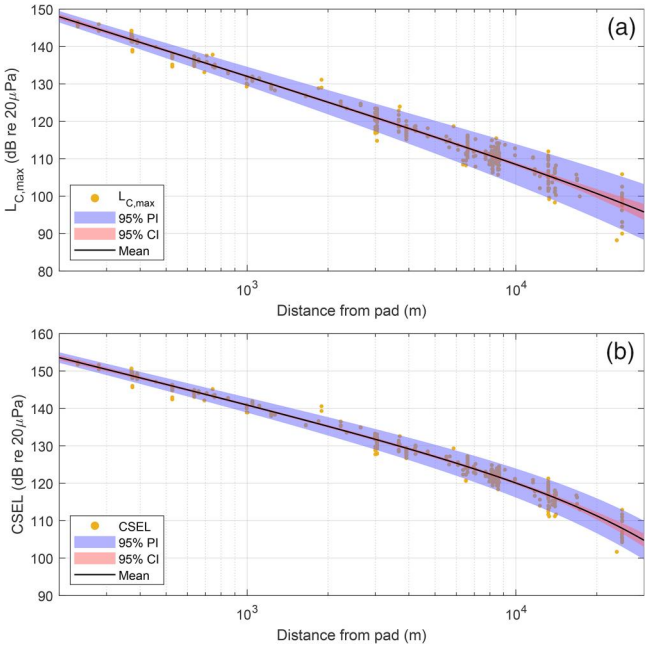


FIG. 5. Figure 3, but for C-weighted metrics.

a quantity that is measurable. It is also closely linked to the decay slope represented by β_1. As Table I shows, β_1 is close to −20 dB per decade for several unweighted maximum-level metrics, consistent with approximate spherical spreading. However, the coefficient should not be interpreted as purely geometric spreading, particularly for SEL because the metric integrates over the entire launch event. Additionally, for $L_{Z,max}$ β_2 is closer to −22 dB per decade, similar to measured acoustic-shock decay and consistent with weak-shock behavior for gaseous explosions (Young *et al.*, 2015) and other observed rocket behavior (Mathews and Gee, 2025). Finally, the linear decay coefficient β_2 introduces curvature in the level versus log-distance decay at large ranges and can be expressed as a level change in decibels per meter. Its form resembles an attenuation coefficient used in atmospheric absorption models (Bass *et al.*, 1995; ANSI, 1995) or propagation through foliage (Attal and Dauchez, 2025). The fitted coefficient alone, however, does not identify which physical mechanisms produce the observed attenuation. Nonetheless, if $\beta_2 = -6.3 \times 10^{-5}$ dB/m for $L_{Z,max}$ were assumed to be dominated by atmospheric absorption, this value would be comparable to the attenuation coefficient at 50 Hz for an ambient temperature of 12 °C, relative humidity of 85%, and ambient pressure of 1 atm. Thus, the values for β_2 are on the order of low-frequency absorption coefficients in the atmosphere, with the A-weighted coefficients being larger (emphasizing higher frequencies) than the Z-weighted coefficients, and the C-weighted coefficients falling between the two.

B. Comparison of coefficient and parameter values between models

The values for these coefficients and parameters found in Table I vary between models. This variation can be

27 October 2026 16:38:30

interpreted based on the nature of the metric being modeled. The logarithmic slope coefficient β_1 varies little between different weightings of L_{max} metrics and strongly resembles spherical spreading as previously mentioned. Irrespective of weighting, SELs decay slower than their L_{max} counterparts due to the integrated nature of the metric. A microphone passes through the angle of maximum acoustic radiation relative to the rocket slower at longer ranges causing an integration to decay slower than spherical spreading. The evidence of this mechanism however is diminished in metrics that emphasize high-frequency content due to spectral shifts in rocket noise at range. As observed by Kellison *et al.* (2023) and Anderson (2026), the peak frequency of rocket noise notably decreases as distance increases. This causes frequency-weighted metrics to progressively deemphasize a larger fraction of the radiated energy. For this reason, the unweighted ZSEL which is influenced by all frequencies has the smallest β_1 while CSEL and ASEL which ignore frequencies that progressively become more dominant at large distances have larger β_1 values.

Variation in the linear decay coefficient β_2 can be attributed to frequency weighting. Within both the L_{max} and SEL metric families Z-weighting has the lowest β_2 followed by C- and A-weighting. This is consistent with the relatively weak atmospheric absorption of low frequencies which influence Z-weighting the most due to the low-frequency content of launch noise. In contrast, metrics with greater high-frequency emphasis generally exhibit larger linear decay terms. Another pattern in the linear decay coefficient found when comparing models is that β_2 values for L_{max} models are smaller than their SEL counterparts except for $L_{A,max}$ and ASEL. No simple physical explanation is apparent for this behavior, and it serves as a reminder that the fitted coefficients arise from an empirical model. While broad trends are physically interpretable, individual coefficients should not be over-interpreted in isolation. However, a lack of direct physical interpretation for the behavior of all coefficients does not diminish the general importance of this analysis, as these coefficients serve as an excellent baseline to which other rocket datasets can be compared.

Variation in the random-effect standard deviation, σ_{cluster}, seems to be sensitive to high-frequency emphasis. Unweighted and C-weighted metrics exhibit similar cluster variability, while A-weighted metrics have nearly double the magnitude.

Variation in the exponent δ also seems to be attributed mostly to frequency weighting. Within a given frequency weighting, L_{max} and SEL exhibit similar values of δ, suggesting that the growth of uncertainty with range is primarily controlled by propagation effects rather than metric integration. Across weightings, a clear trend is observed: unweighted metrics exhibit the slowest growth in variability, followed by C-weighted metrics, with A-weighted metrics showing the most rapid increase. This behavior is consistent with the greater susceptibility of high-frequency sound to changes in propagation path and atmospheric conditions at large ranges.

VI. EXTERNAL EVALUATION OF THE MODEL

The model form and coefficients presented in this paper were derived exclusively from Falcon 9 noise measurements collected at VSFB. Although Falcon 9 is currently one of the most frequently launched orbital vehicles, it is not the only active launch vehicle, nor is VSFB the only spaceport supporting Falcon 9 orbital operations. It is therefore important to evaluate whether elements of the distance-dependent behavior identified for Falcon 9 at VSFB may generalize to other vehicles and other launch environments.

This section examines two external applications. First, the logarithmic decay behavior of Falcon 9 is compared to published measurements of Starship Super Heavy to assess whether slope characteristics may be transferable to other vehicle classes. Second, Falcon 9 launches conducted from Cape Canaveral Space Force Station (CCSFS) and Kennedy Space Center (KSC) are evaluated using the VSFB-derived model to examine geographic transferability. Together, these analyses provide insight into which aspects of the model structure may generalize beyond the original dataset and which require vehicle- or site-specific calibration.

A. Model slope comparison to Starship Super Heavy Flight 6

To evaluate whether aspects of the distance-dependent behavior identified for Falcon 9 are applicable to other launch vehicles, logarithmic decay rates reported for Starship Super Heavy Flight 6 (Gee *et al.*, 2025a) were compared to the fitted β_1 coefficients derived for Falcon 9. The comparison includes $L_{Z,max}$, $L_{A,max}$, ZSEL, and ASEL. Using 12 measurements between 1 and 10 km from the launch pad, the published Starship noise levels were fit with a simple linear model in $\log_{10}(r)$ to estimate the logarithmic decay rates presented in Table III.

Agreement between vehicles is strongest for the unweighted maximum level, $L_{Z,max}$. The Falcon 9 and Starship slopes differ by 1.4 dB per decade increase in distance, a difference that is small relative to measurement variability and differences in modeling structure. This close correspondence suggests that the logarithmic decay behavior of unweighted maximum levels may be broadly applicable across vehicles despite substantial differences in thrust and scale.

Within each vehicle, $L_{A,max}$ and ASEL exhibit nearly identical logarithmic decay rates, and the separation between $L_{Z,max}$ and ZSEL slopes is comparable for Starship Super Heavy and Falcon 9 (3.8 and 5.3 dB per decade,

TABLE III. Comparison of logarithmic decay coefficients β_1 for Falcon 9 and Starship Super Heavy across selected acoustic metrics.

Metric	Falcon 9	Starship Super Heavy
$L_{Z,max}$	−21.8	−23.2
$L_{A,max}$	−21.8	−24.9
ZSEL	−16.5	−19.4
ASEL	−21.1	−24.7

27 October 2026 16:38:30

https://doi.org/10.1121/10.0046889

respectively). These consistent internal relationships indicate that relative behavior among metrics is structurally similar across vehicles.

Differences observed in the weighted metrics are plausibly influenced by spectral content. Starship Super Heavy operates at substantially higher thrust and with a larger effective nozzle diameter than Falcon 9 (Gee *et al.*, 2025b), conditions associated with differences in source spectrum. Because A-weighted metrics apply frequency-dependent corrections, variations in spectral shape are expected to influence their apparent decay rates. Starship has a one-third-octave peak frequency half that of Falcon 9 at comparable distances according to work by Mathews *et al.* (2021) and Gee *et al.* (2025b), causing a larger portion of its noise to be deemphasized by A-weighting. The larger magnitude slopes observed for $L_{A,max}$ and ASEL for Starship are therefore consistent with expected spectral differences rather than fundamentally different propagation behavior.

One notable discrepancy is the approximately 3-dB-per-decade difference in ZSEL decay rate. Unlike the weighted metrics, ZSEL is not directly influenced by frequency weighting, making this difference less readily attributable to spectral differences. The origin of this deviation is not immediately clear and additional measurements across vehicles would help clarify this behavior.

For additional context, published Atlas V measurements reported by Mathews and Gee (2025) indicate a logarithmic decay rate for $L_{Z,max}$ between approximately –20 and –22 dB per decade over distances from 200 m to 7 km (Mathews *et al.*, 2023). This range closely aligns with the Falcon 9 value and supports the observation that unweighted maximum levels for medium-lift vehicles exhibit similar distance-dependent decay behavior.

Taken together, these comparisons indicate that the logarithmic distance dependence of unweighted maximum levels is similar across the vehicles considered, while weighted metrics show greater sensitivity to vehicle-specific spectral content. The ZSEL discrepancy remains unresolved. These results support transferring the model form as a hypothesis for other launch vehicles but not transferring Falcon 9 coefficients without additional calibration data.

B. Florida launches

Additional Falcon 9 measurements were collected by BYU for eight missions launched from CCSFS and KSC. These measurements were obtained using the same instrumentation and processing methods employed at VSFB. In total, 39 waveforms were used to calculate the same acoustic metrics modeled in the VSFB dataset. Measurement distances ranged from approximately 700 m to 20 km from the launch pad.

A comparison between the Florida measurements and the Falcon 9 mean curves, confidence intervals, and prediction intervals derived from the VSFB dataset are displayed for Z- and A-weighted metrics in Fig. 6 and Fig. 7. For all metrics, all but 2 (∼5%) of the Florida measurements fall within the 95% prediction intervals calculated from VSFB data. This indicates that the VSFB-derived model captures the overall range of expected variability even when applied to a different launch site. Additional measurements made by other labs at CCSFS and KSC also fall in the 95% prediction interval described here (Williams *et al.*, 2025).

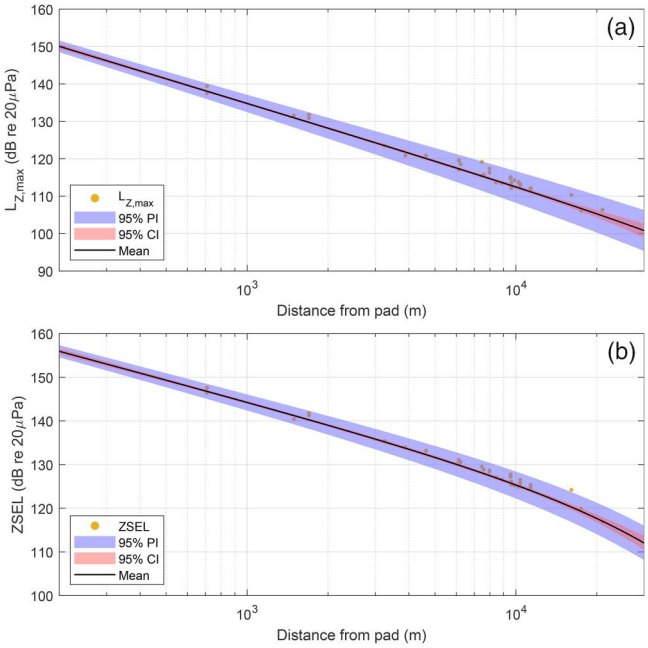


FIG. 6. The 39 $L_{Z,max}$ (a) and ZSEL (b) data points calculated from Falcon 9 launch recordings at CCSFS and KSC, along with the modeled mean levels and the associated $CI_{95\%}$ and $PI_{95\%}$ from the VSFB model.

Although most Florida measurements fall within the VSFB prediction intervals, many are systematically higher than the VSFB mean curves. Although there are insufficient data to assess a site-dependent difference in mean level, future work could evaluate atmospheric conditions, terrain,

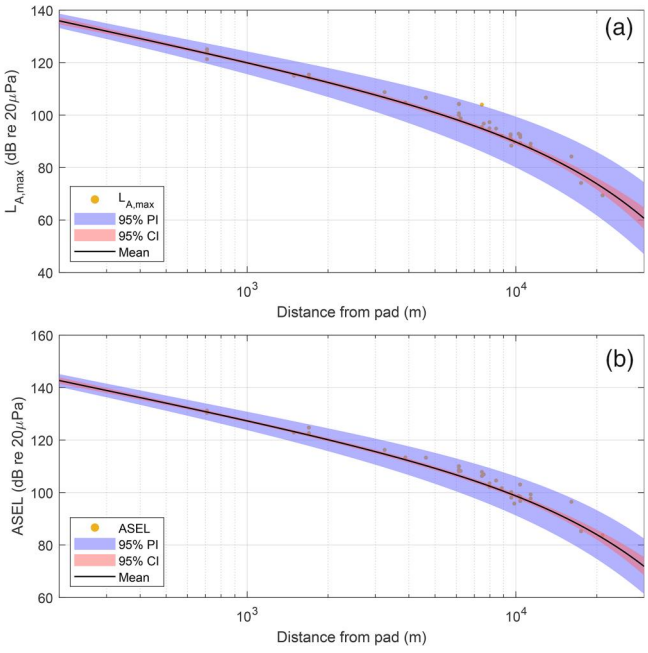


FIG. 7. Figure 6, but for A weighting.

27 October 2026 16:38:30

ground impedance, and trajectory to identify long-range differences in metric decay between launches from the two coasts.

The A-weighted metrics in Fig. 7 suggest similar findings: an overall reproduction of the same geometric decay and long-range additional losses, and a potential increase in levels with respect to the VSFB-modeled mean. The agreement supports the portability of the model form across launch sites, while the offset indicates that site-specific calibration may be needed for the mean level.

VII. EFFECTS OF TERRAIN SHIELDING

Distance from the launch pad is the dominant predictor of mean acoustic level in the statistical model, but local terrain can produce systematic departures when it blocks the line of sight to the source. Mathews *et al.* (2021) documented a Falcon 9 pressure waveform measured in a canyon more than 13 km from the pad in which an increase in running sound pressure level coincided with the vehicle clearing the canyon walls. VSFB contains rugged terrain with steep canyons, making terrain shielding a relevant exception to a purely distance-based description. To better quantify the magnitude of this effect, a paired-site analysis was conducted at two locations with similar distance and azimuth but markedly different terrain exposure.

A. Paired-site design

Five Falcon 9 launches were measured at two fixed locations approximately 3 km downrange from the launch pad (see Fig. 8). Recorder 1 is on elevated terrain with line of sight to the launch vehicle during peak acoustic emission, whereas Recorder 2 is located within a canyon and is shielded from the vehicle during the estimated peak-radiation angle. The source-observer geometry was evaluated using the vehicle directivity angle reported by Mathews *et al.* (2021). The two sites have closely matched distances and azimuths, and both were measured during the same launches, allowing the paired comparison to control for launch-to-launch variability while isolating the effect of terrain shielding.

B. Statistical results

Across all five paired recordings and all six acoustic metrics, measurements at the shielded site were generally lower than those measured at the unshielded site. The sole exception occurred for a single $L_{A,max}$ pairing in which the shielded recorder measured 0.4 dB higher. Aside from this isolated case, terrain shielding consistently reduced measured acoustic levels. An example of the paired differences is shown for $L_{Z,max}$ in Fig. 9 where the mean reduction due to terrain shielding is 3 dB. While the magnitude of the reduction varies from launch to launch, the presence of terrain shielding produces a clear downward shift in the mean $L_{Z,max}$ level at the canyon site. Mean, maximum, minimum, and range of the shielding-induced changes are summarized in Table IV.

Within both the L_{max} and SEL metric families, the mean magnitude of shielding-induced reduction for a given metric depends strongly on frequency weighting. Weighted

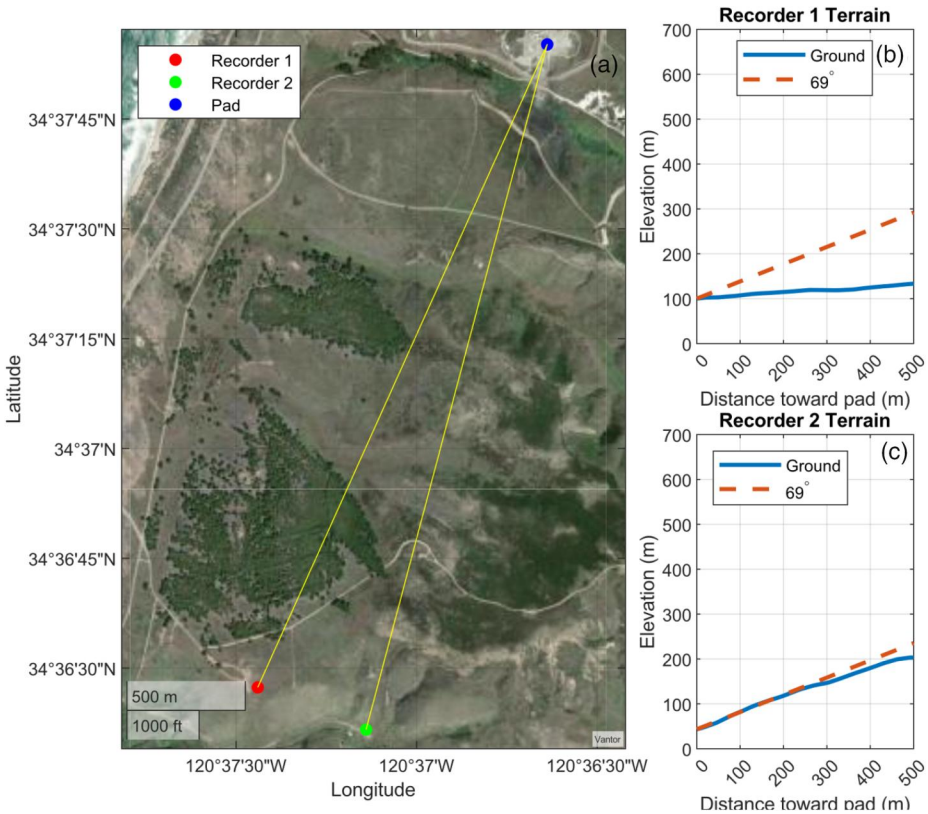


FIG. 8. The large pane on the left shows the location of Recorder 1 and 2 relative to Falcon 9's launch pad at VSFB, each 3 km away. The two panes to the right show estimated lines-of-sight to the rocket at the angle of maximum acoustic radiation around 69°. Notice for Recorder 2 in the bottom right this line of sight intersects with the ground.

27 October 2026 16:38:30

https://doi.org/10.1121/10.0046889

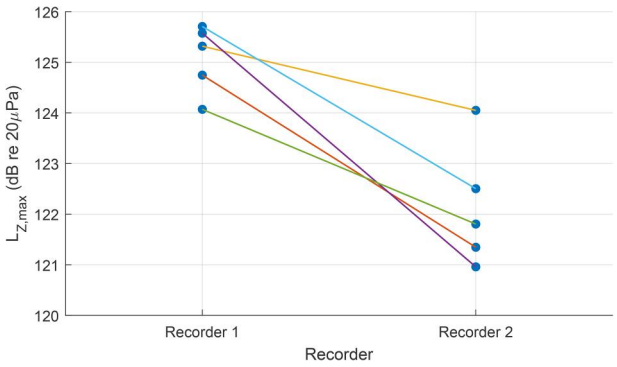


FIG. 9. $L_{Z,max}$ compared between 5 Falcon 9 launches at Recorders 1 and 2. Lines connect measurements taken during the same launch.

metrics, particularly A-weighted metrics, show larger mean reductions than their unweighted counterparts. This pattern is consistent with terrain preferentially attenuating higher-frequency content, which diffracts less efficiently around large topographic features. The range of observed shielding effects also increases with weighting: Z-weighted metrics show the smallest range, C-weighted metrics are intermediate, and A-weighted metrics show the largest range. This ordering suggests that the spectral content most emphasized by A-weighting is also the most variable in the presence of terrain shielding.

The response also differs between the L_{max} and SEL families because the metrics represent different aspects of the event. For a given weighting, SEL generally shows a smaller range of shielding-induced changes than the corresponding L_{max} metric, consistent with the smoothing effect of temporal integration. Mean reductions differ by weighting: for unweighted metrics, the reduction in $L_{z,max}$ is larger than that in ZSEL, whereas for the weighted metrics, SEL shows larger mean reductions than the corresponding L_{max} metrics. The present dataset does not provide a sufficient basis for explaining this difference, but it identifies a potentially useful direction for future study.

The terrain results suggest a possible future improvement to the distance-based model by incorporating terrain exposure, but they do not justify a general correction factor. The paired sites represent an extreme shielding geometry that is relatively uncommon at launch facilities, and the sample size is small. The more general result is that all metrics were sensitive to shielding, with larger mean reductions for weighted metrics and the largest reductions for the integrated weighted metrics. SEL metrics also showed smaller launch-to-launch ranges in the shielding effect, consistent with their temporal integration.

TABLE IV. Summary of changes in acoustic metrics comparing a recorder that has line-of-sight to the rocket at the angle of maximum acoustic radiation to one that does not. Negative values indicate that the metric was lower for the shielded recorder.

Metric	Mean	Maximum	Minimum	Range
$L_{Z,max}$	−3	−4.6	−1.3	−3.3
$L_{A,max}$	−3.5	−6.3	0.4	−6.7
$L_{C,max}$	−2.9	−5.1	−0.9	−4.2
ZSEL	−2.5	−3.4	−2.1	−1.4
ASEL	−5.1	−7.4	−3.1	−4.3
CSEL	−3.4	−4.6	−2.6	−2.1

VIII. CONCLUSION

The distance from the launch pad is a strong first-order predictor of L_{max} and SEL for Falcon 9 launches across all weighting schemes considered. Using 401 observations spanning approximately 200 m to 30 km, a mixed-effects model with logarithmic and linear distance terms, a cluster-level random intercept, and a power-law variance structure captures the dominant mean trends and the observed increase in variability with distance. The fitted coefficients provide a reproducible description of the mean response, confidence intervals for the mean, and prediction intervals for individual observations.

The logarithmic coefficients for L_{max} are generally close to, but slightly steeper than, spherical spreading, while the linear distance term captures additional long-range deviation from power law geometric spreading, especially for A-weighted metrics. The power-law variance structure represents the observed increase in measurement variability with distance. Together, these components provide a compact statistical description of both the mean response and the distribution of individual measurements.

Comparison with Starship Super Heavy Flight 6 indicates that the logarithmic decay behavior of unweighted maximum level is similar across the two vehicles: the fitted slopes differ by only 1.4 dB per decade. The weighted metrics show larger differences, consistent with differences in source spectra, and the ZSEL discrepancy remains unexplained. Applying the VSFB model to Falcon 9 measurements from Cape Canaveral Space Force Station and Kennedy Space Center further shows that the model form remains useful across launch sites. Although Florida measurements are systematically elevated relative to the VSFB mean, most fall within the VSFB prediction intervals, indicating that the model captures a substantial portion of the observed cross-site variability.

The terrain analysis demonstrates that strong shielding can produce systematic level reductions that are not captured by distance alone. These effects are more prominent for L_{max} than SEL metrics. In contrast, seasonal and diurnal effects were small relative to other sources of variability and did not materially improve predictive capability for the present dataset.

These results provide a statistical reference for environmental assessment and for evaluation of launch-noise prediction models. The distance-based mean curves provide expected levels as a function of range, while the prediction intervals quantify the substantial spread of individual measurements, which increases with distance. The model therefore supports comparison among launch sites and vehicles and provides a measured benchmark against which physics-

27 October 2026 16:38:30

based or semi-empirical prediction methods can be evaluated.

Future work should expand the dataset to additional launches, vehicles, and spaceports. Additional Starship measurements across multiple flights would help resolve the observed ZSEL discrepancy and strengthen cross-vehicle comparisons. Combining empirical fits with physics-based propagation modeling may also improve understanding of terrain shielding, nonlinear propagation, and spectral evolution with distance. Finally, the prediction intervals remain wide, particularly at long range. Future analyses should examine whether weather, trajectory, terrain, and other propagation variables can explain a meaningful fraction of this variability and thereby improve predictive performance.

ACKNOWLEDGMENTS

This work was funded by VSFB and US Army Corps of Engineers. We thank VSFB for supporting measurement logistics and numerous BYU and CSUB students who contributed to data collection.

AUTHOR DECLARATIONS

Conflict of Interest

The authors have no conflict of interest to report for this work.

DATA AVAILABILITY

Compiled data that are used to produce the figures in this paper are available upon request to the corresponding author.

Akaike, H. (**1974**). "A new look at the statistical model identification," IEEE Trans. Autom. Control **19**(6), 716–723.

Anderson, M. C. (**2026**). "Sonic booms from rockets: Measurements and modeling," Ph.D. dissertation, Brigham Young University, Provo, UT.

Anderson, M. C., Gee, K. L., Novakovich, D. J., Mathews, L. T., and Jones, Z. T. (**2022**). "Comparing two weather-robust microphone configurations for outdoor measurements," Proc. Meet. Acoust. **42**(1), 040005.

Anderson, M. C., Stephenson, J. H., Zawodny, N. S., and Gee, K. L. (**2021**). "Characterizing the effects of two ground-based outdoor microphone configurations," Proc. Meet. Acoust. **39**(1), 055011.

Ang, L. P., Kong, F., Hernandez-Rodriguez, E., Liu, Q., Cerrejon, C., Feldman, M. J., Shu, L., Ye, L., Gao, L., Ang, L. L., and Yin, X. (**2024**). "Rocket launches threaten global biodiversity conservation," Commun. Earth Environ. **5**, 799.

ANSI (**1995**). S1.26, *Calculation of the absorption of sound by the atmosphere*.

Attal, E., and Dauchez, N. (**2025**). "Acoustic performance of foliage based on green systems at normal incidence," Appl. Acoust. **234**, 110591.

Bass, H. E., Sutherland, L. C., Zuckerwar, A. J., Blackstock, D. T., and Hester, D. M. (**1995**). "Atmospheric absorption of sound: Further developments," J. Acoust. Soc. Am. **97**(1), 680–683.

Casiano, M. J. (**2024**). "Liftoff environments overview," *NASA NTRS Document 20240000001* (Marshall Space Flight Center Redstone Arsenal, United States).

Christian, M. A., Gee, K. L., and Olaveson, T. (**2023**). "Connecting the convective Mach number to full-scale supersonic jet noise directivity," AIAA 2023-3351.

Cunningham, C., Anderson, M. C., Moats, L. T., Gee, K. L., Hart, G. W., and Hall, L. K. (**2023**). "Acoustical measurement and analysis of an Atlas V launch," Proc. Meet. Acoust. **46**(1), 045005.

Eldred, K. M. (**1971**). "Acoustic Loads Generated by the Propulsion System," NASA SP-8072, Washington, DC.

FAA (**2022**). "Fundamentals of noise and sound: Noise metrics," https://www.faa.gov/regulations_policies/policy_guidance/noise/basics#metrics (Last viewed April 6, 2026).

FAA (**2024**). "FAA aerospace forecast fiscal years 2024–2044," *Aerospace Forecast FY2024-2044* (Federal Aviation Administration, Washington, DC).

FAA (**2025**). *Adoption of the Environmental Impact Statement and Record of Decision for Authorizing Changes to the Falcon Launch Program for Vandenberg Space Force Base*, California (Office of Commercial Space Transportation, Washington, DC).

FAA, Department of the Air Force, United States Coast Guard, and National Aeronautics and Space Administration (**2025**). "Final environmental assessment: SpaceX Falcon 9 operations at Space Launch Complex 40, Cape Canaveral Space Force Station, Florida," EAXX-021-12-000-1737545438 (Washington, DC).

Gee, K. L., Lubert, C. P., and James, M. M. (**2024**). "The roar of a rocket," Phys. Today **77**(3), 46–47.

Gee, K. L., Pulsipher, N. L., Kellison, M. S., Hart, G. W., Mathews, L. T., and Anderson, M. C. (**2025a**). "Starship super heavy acoustics: Comparing launch noise from flights 5 and 6," JASA Express Lett. **5**(2), 023602.

Gee, K. L., Pulsipher, N. L., Kellison, M. S., and Hart, G. W. (**2025b**). "Measuring the world's most powerful rocket: Noise from Starship Super Heavy," in *Proceedings of ACOUSTICS 2025: Sounds of the Sunset Coast, Joondalup*, Western Australia, November 12–14, 2025 (Australian Acoustical Society Toowong DC QLD, 2025), pp. 19–26.

Guest, S. H., and Slone, R. M., Jr. (**1972**). "Structural damage claims resulting from acoustic environments developed during static test firing of rocket engines," in *NASA Space Shuttle Technology Conference: Dynamics and Aeroelasticity; Structures and Materials*, San Antonio, TX, April 12–14, 1972 (NASA, Houston, TX), NASA NTRS Document ID 19720023218.

Hart, G. W., Mathews, L. T., Anderson, M. C., Durrant, J. T., Bassett, M. S., Olausson, S. A., Houston, G., and Gee, K. L. (**2022**). "Methods and results of acoustical measurements made of a Delta IV Heavy launch," Proc. Mtgs. Acoust. **45**(1), 040003.

IEC (**2013**). 61672-1, *Electroacoustics—sound level meters—part 1: Specifications* (International Electrotechnical Commission, Geneva, Switzerland).

ISO (**2016**). 1996-1, *Acoustics—description, measurement and assessment of environmental noise, part 1: Basic quantities and assessment procedures* (International Organization for Standardization, Geneva, Switzerland).

Kellison, M. S., Gee, K. L., Cunningham, C. F., Coyle, W. L., Moore, T. R., and Hart, G. W. (**2023**). "Community-based noise measurements of the Artemis-I mission," Proc. Meet. Acoust. **51**(1), 040004.

Kellison, M. S., Gee, K. L., and Hart, G. W. (**2026**). "Falcon 9 noise characterization from two measurement campaigns," AIAA/CEAS 2026-3443.

Larson Davis (**2025**). "SoundAdvisor Model 831C—User's Manual," Provo, UT.

Lubert, C. P., Gee, K. L., and Tsutsumi, S. (**2022**). "Supersonic jet noise from launch vehicles: 50 years since NASA SP-8072," J. Acoust. Soc. Am. **151**(2), 752–791.

Mathews, L. T., Anderson, M. C., Gardner, C. D., McLaughlin, B. W., Hinds, B. M., McCullah-Boozer, M. R., Hall, L. K., and Gee, K. L. (**2023**). "An overview of acoustical measurements made of the Atlas V JPSS-2 rocket launch," Proc. Meet. Acoust. **51**(1), 040003.

Mathews, L. T., and Gee, K. L. (**2025**). "Methods for predicting overall sound power and maximum overall sound pressure levels from heated supersonic jets, including rockets," J. Acoust. Soc. Am. **158**(1), 371–379.

Mathews, L. T., Gee, K. L., and Hart, G. W. (**2021**). "Characterization of Falcon 9 launch vehicle noise from far-field measurements," J. Acoust. Soc. Am. **150**(1), 620–633.

Mathews, L. T., Gee, K. L., Hart, G. W., Rasband, R. D., Novakovich, D. J., Irarrazabal, F. I., Vaughn, A. B., and Nelson, P. (**2020**). "Comparative analysis of noise from three Falcon 9 launches," J. Acoust. Soc. Korea **39**(4), 322–330.

McDowell, J. C. (**2026**). "Orbital launch log," https://planet4589.org/space/gcat/data/derived/launchlog.html (Last viewed February 10, 2026).

27 October 2026 16:38:30

McInerny, S. A. (**1992**). "Characteristics and predictions of far-field rocket noise," Noise Control Eng. J. **38**(1), 5–16.
McInerny, S. A., Francine, J. K., Stewart, B. S., and Thorson, P. H. (**1997**). "The influence of low-frequency instrumentation response on rocket noise metrics," J. Acoust. Soc. Am. **102**(5), 2780–2785.
Moats, L. T. (**2026**). "Collecting and analyzing Falcon 9 launch noise from Vandenberg Space Force Base," Master's thesis, Brigham Young University, Provo, UT.
NASA (**2026**). "Nasa commercial crew program: Overview and essentials," https://www.nasa.gov/humans-in-space/commercial-space/commercial-crew-program (Last viewed February 11, 2026).
NIOSH (**1998**). 98-126: *Criteria for a recommended standard: Occupational noise exposure* (National Institute for Occupational Safety and Health, Washington, DC).
OECD (**2019**). *The Space Economy in Figures: How Space Contributes to the Global Economy* (OECD, Paris).
OECD (**2023**). *The Space Economy in Figures* (OECD, Paris).
OSHA (**2008**). 29 CFR 1910.95: *Occupational noise exposure* (Occupational Safety and Health Administration, Washington, DC).
Pilger, C., Hupe, P., Gaebler, P., and Ceranna, L. (**2021**). "1001 rocket launches for space missions and their infrasonic signature," Geophys. Res. Lett. **48**, e2020GL092262, https://doi.org/10.1029/2020GL092262 .
Pulsipher, N. L., Gee, K. L., Hart, G. W., and Hall, L. K. (**2024**). "Far-field acoustic variability across twelve Falcon 9 launches near Vandenberg Space Force Base," Proc. Meet. Acoust. **54**(1), 040015.
SpaceX (**2025**). "Falcon Payload User's Guide," https://www.spacex.com/assets/media/falcon-users-guide-2025-05-09.pdf (Last viewed February 11, 2026).
Williams, H. N., Coyle, W. L., and Gee, K. L. (**2025**). "RUMBLE as a tool for community spaceport noise prediction," Proc. Mtgs. Acoust. **60**(1), 040009.
Young, S. M., Gee, K. L., Neilsen, T. B., and Leete, K. M. (**2015**). "Outdoor measurements of spherical acoustic shock decay," J. Acoust. Soc. Am. **138**(3), EL305–EL310.

27 October 2026 16:38:30